

Manuscript version: Author's Accepted Manuscript

The version presented in WRAP is the author's accepted manuscript and may differ from the published version or Version of Record.

Persistent WRAP URL:

<http://wrap.warwick.ac.uk/129303>

How to cite:

Please refer to published version for the most recent bibliographic citation information. If a published version is known of, the repository item page linked to above, will contain details on accessing it.

Copyright and reuse:

The Warwick Research Archive Portal (WRAP) makes this work by researchers of the University of Warwick available open access under the following conditions.

Copyright © and all moral rights to the version of the paper presented here belong to the individual author(s) and/or other copyright owners. To the extent reasonable and practicable the material made available in WRAP has been checked for eligibility before being made available.

Copies of full items can be used for personal research or study, educational, or not-for-profit purposes without prior permission or charge. Provided that the authors, title and full bibliographic details are credited, a hyperlink and/or URL is given for the original metadata page and the content is not changed in any way.

Publisher's statement:

Please refer to the repository item page, publisher's statement section, for further information.

For more information, please contact the WRAP Team at: wrap@warwick.ac.uk.

Shape Memory and Self-healing Behavior of SBS/EMAA Elastomers Containing Ionic Interactions

Wenjing Wu,^{1,2} Yutao Zhou,¹ Jie Li,² and Chaoying Wan*¹

¹International Institute for Nanocomposites Manufacturing (IINM), WMG, University of Warwick, CV4 7AL, UK

²Aerospace Research Institute of Materials & Processing Technology, 100076, Beijing, China

Email: Chaoying.wan@warwick.ac.uk

Abstract

Ionic interactions were introduced to styrene-butadiene-styrene (SBS) through blending with ethylene-methacrylic acid copolymer (EMAA) and zinc oxide (ZnO), and a following *in situ* neutralization reaction between the carboxyl groups of EMAA and ZnO. The resultant SBS/EMAA (60/40 wt%) blends containing zinc carboxylate crosslinks **exhibited high modulus and strong long-time relaxation characteristics**. With 74% of the carboxyl groups neutralized (zinc cation fraction of 1.7 wt%), the tensile strength of the blends was increased from 14.6 MPa to 16.6 MPa, and the stress at 100% extension was increased from 4.8 MPa to 8.1 MPa. The melting temperature of EMAA was utilized to trigger the shape memory behavior of SBS/EMAA, and the reversible ionic bonds endowed SBS with better shape memory and self-healing performance. **The shape-fixing ratio and recovery ratio of SBS were increased from 90.2% and 56.5% up to 93.3% and 84.2%, respectively**. When the cut surfaces of SBS/EMAA/Zn samples were brought back into contact and annealed at 100 °C for 1 h, the strength and the elongation at break were recovered by 36% and 21%, respectively. **This introduction of ionic interactions** through the EMAA-ZnO neutralization reactions imparts new functions to SBS thermoplastic elastomers.

1. Introduction

Self-healing behavior of polymers originates from the dynamic or quasi-dynamic interactions, involving dynamic covalent bonds such as **Diels-Alder bonds or disulphide bonds**, supramolecular interactions such as ionic, π - π , intermolecular electrostatic attraction, hydrogen bonding, and metal-ligand coordination, as well as molecular chain entanglements^[1, 2].

Ionic interactions can be introduced into rubbers through **the ion-dipole interactions among the ionisable groups** of polymer chains such as carboxylate, sulfonate and phosphonate. The aggregation of the ionic clusters acts as physical crosslinks responsible for enhanced flexibility, toughness, temperature-sensitivity and potential self-healing function^[1-5]. When ionic compounds, such as zinc dimethacrylate were **introduced into** natural rubbers^[6], or were formed *in situ*^[7] through a well-controlled peroxide induced graft-polymerization, the resultant ionic crosslinks form **a reversible supramolecular crosslinking network** in the rubber matrix and lead to a nearly **complete** recovery of the mechanical properties after a self-healing process.

Non-metallic cations can also be introduced to rubber matrix to form ionic crosslinks. When some nitrogen-containing compounds, such as alkylimidazoles^[3, 8, 9], 4-ethyl-4-methylmorpholinium methylcarbonate^[10] and 2-(dimethyl amino)-ethyl methacrylate^[11] were introduced into poly(isobutylene-co-isoprene) rubber or acrylate rubber, excellent mechanical and self-healing performance were obtained, e.g., a healed tensile strength of 10.7 MPa (healing efficiency of 74%) and a elongation at break of 1040% (healing efficiency of 98%)^[3].

In addition to forming an ionic crosslinking network, metal ions can also be utilised to form supramolecular networks through metal-ligand interactions^[12, 13] in rubber matrix.

For rubbers with functional groups, such as carboxylated styrene butadiene rubber (XSBR), the ionic interactions can be introduced by adding metal oxides^[14] or amino compounds^[15], to

enable self-healing and simultaneously improve the mechanical properties. For saturated rubbers, the ionic interactions can be introduced by blending with functional polymers or ionomers, such as acrylic acid based copolymers. In fact, the acrylic acid based copolymers and their ionomers have good self-healing capability at elevated temperatures^[1, 16]. When epoxidized natural rubber was blended with ionomers of ethylene acrylic acid^[17-19], the blends exhibited good self-healing and shape memory performance^[20].

Styrene-butadiene-styrene copolymer (SBS) contains microphase-separated microstructures where the styrene blocks aggregate as the hard domains and act as physical crosslinking points, the butadiene blocks present as the soft domains and provide the flexibility and toughness. The physical crosslinks enable SBS to behave like an elastomer but can be processed as a thermoplastic, which has expanded its applications to wide fields such as automobiles, electronics, medical equipment, sports materials and shoes. SBS doesn't exhibit self-healing behavior despite the physically crosslinked structures provided by π - π stacking interactions and the strong molecular entanglements from the butadiene soft segments. In this study, ethylene-methacrylic acid copolymer (EMAA) was introduced to SBS to create ionic bonds in the blends. The ionic interactions are formed between the carboxyl groups of EMAA and zinc oxide particles. The microstructures and *in situ* neutralization reactions were characterised, and the effect of the ionic interactions on the self-healing and shape memory behaviors of SBS were investigated. It demonstrates that the coupling of non-covalent interactions such as ionic interactions and hydrogen interactions can tune the polymer chain relaxation characteristics and generate new properties.

2. Experimental Section

2.1. Materials

Styrene-butadiene-styrene copolymer (SBS, Vector® 8508A) with 71 wt% butadiene, the melt flow rate of 12 g/10 min (200 °C, 5kg) and the Shore A hardness of 67, was purchased from Dexco,. Ethylene-methacrylic acid copolymer (EMAA, Nucrel® 925) containing 15 wt% of methacrylic acid, with the melt flow rate of 25 g/10 min (190°C, 2.16kg), was kindly provided by Dow Ltd. Zinc oxide (ZnO) was purchased from Zochem, Inc.

2.2. Sample Preparation

SBS/EMAA (60/40 wt%) blends were prepared with a Haake Rheometer at a rotor speed of 60 rpm at 170 °C. EMAA was firstly melt in the mixing chamber for 1 min, followed with the SBS addition. After 1 min, ZnO power was added and further mixed for 8 min to obtain the blends. Based on the methacrylic acid content of the SBS/EMAA blends, the theoretical ZnO concentration for a complete neutralization of the acid in the blend was calculated to be 2.84 wt% of the blend. A range of ZnO concentration was added from 0.5, 1.0, 1.5, 2.5 and 5.0 times of 2.84 wt% in order to optimize the ionic bond concentrations. The blends were further compression-molded at 190 °C under 10 MPa for 20 min to complete the neutralization reaction. The blends are denoted as SBS/EMAA/Zn (x), where x is varied from 0.5, 1.0, 1.5, 2.5 to 5.0, representing the concentration of the ZnO. The blends obtained were used for structural analysis and mechanical, rheological and self-healing characterizations.

2.3. Characterization

The tensile testing, stress relaxation, cyclic tensile and shape memory performance were performed using a Shimadzu Autograph AGS-X tester equipped with an oven, with samples conforming to ASTM-D638-14 type V. For tensile testing, the extension rate was 50 mm min⁻¹ with a 10 kN load cell, and the tests were carried out at room temperature according to ASTM-D638. During the stress relaxation experiments performed at room temperature, the specimen

was stretched to 100% strain at the extension rate of 50 mm min^{-1} and the constant strain was maintained to measure the stress relaxation for 30 min. During the cyclic tensile experiments, **one specimen was tested for each sample**, and in each cycle, the specimen was stretched to 200% strain and then unloaded to 0 strain at 10 mm min^{-1} . After the first cycle, the specimen was relaxed at room temperature for a certain waiting time (0, 10 min) prior to the subsequent two cycles. Before the last cycle, the specimen was heated and isothermal for 30 min at $100 \text{ }^\circ\text{C}$, and then cooled and isothermal for 30 min at $25 \text{ }^\circ\text{C}$. The shape memory experiments were conducted in a strain-controlled mode. The specimen was firstly heated to $80 \text{ }^\circ\text{C}$ and maintained at this temperature for 5 min, and then was stretched to the fixing strain of 40% (ε_m) from 0 strain at 50 mm/min . After that, the specimen was cooled to $25 \text{ }^\circ\text{C}$ and maintained at this temperature for 5 min, and then was unloaded. The residual strain is representative of the fixed strain, defined as ε_1 . The specimen was finally heated to $80 \text{ }^\circ\text{C}$ and maintained at this temperature for 5 min to recover the original shape and the final remaining strain was defined as ε_2 . The shape fixity ratio (R_f) and the shape recovery ratio (R_r) were calculated by $R_f = \varepsilon_1/\varepsilon_m$ and $R_r = (\varepsilon_1 - \varepsilon_2)/\varepsilon_1$, respectively.

Fourier transform infrared spectra (FTIR) were collected using Bruker TENSOR 27 at a resolution of 4 cm^{-1} with 32 scans.

Scanning electron microscopy (SEM) images of cryogenically fractured surface of the blends were carried out using a Zeiss SUPRA 55-VP field emission scanning electron microscopy system. The cryogenically fractured surface was etched by tetrahydrofuran to remove the SBS phase prior to testing.

Dynamic mechanical thermal analysis (DMTA) was performed on a Triton 2000 DMA (Triton Technology, Inc.) with samples $20 \text{ mm} \times 5 \text{ mm} \times 1 \text{ mm}$ in tension mode from -120 to $250 \text{ }^\circ\text{C}$ using a temperature ramp of $3 \text{ }^\circ\text{C min}^{-1}$, with 0.05 mm amplitude and a frequency of 1.0 Hz .

Differential scanning calorimetry (DSC) experiments were conducted on a DSC 2910 (TA Instruments, Inc.) with a heating-cooling-heating procedure. All measurements were carried out using a constant heating and cooling rate of $20\text{ }^{\circ}\text{C min}^{-1}$ between 0 and $200\text{ }^{\circ}\text{C}$.

Rheological experiments were performed on a Haake Mars III Rheometer with 25 mm diameter stainless steel parallel plate geometry. Frequency sweep experiments between $100\sim 0.01\text{ Hz}$ were performed at 100, 120, 150, 170, 190 and $210\text{ }^{\circ}\text{C}$, and the gap was 0.8 mm, and a constant shear strain 0.5%, which was within the linear viscoelastic region of the materials according to the strain sweep experiment, was used. The storage modulus (G') and loss modulus (G'') curves with changing frequency were recorded. Taking $150\text{ }^{\circ}\text{C}$ as the reference temperature (T_r), the master curves were obtained using the time-temperature superposition method. The curves were shifted by a horizontal shift factor of a_T and a vertical correction factor of $b_T = \rho_r T_r / (\rho T)$, to achieve the best superposition with data at T_r . **After the horizontal and vertical shift of the curves, the frequency f was changed to $a_T f$, and the moduli G' and G'' were changed to $b_T G'$ and $b_T G''$, respectively.**

Self-healing experiments were performed using standard tensile specimens. The samples were cut 80~90% of the width in the middle of the specimens with a razor blade. Immediately, the cut sections were separated from each other and then pressed together to contact, and the specimens were put into a specimen-sized mold to keep the cut sections contact. In this state, the specimens were allowed to heal for 1 h and one day at $100\text{ }^{\circ}\text{C}$ and then stored at room temperature. The healed specimens were then subjected to tensile testing. The healing efficiency of the strength and elongation at break were calculated as $\sigma(h) / \sigma(o) \times 100\%$ and $\varepsilon(h) / \varepsilon(o) \times 100\%$, respectively, where $\sigma(h)$ and $\varepsilon(h)$ are the tensile strength and elongation at break of the healed specimens, respectively, and $\sigma(o)$ and $\varepsilon(o)$ are the original tensile strength and elongation at break, respectively.

3. Results and Discussion

3.1. Neutralization Reaction of ZnO and EMAA

During the melt-mixing process, the ZnO can potentially react with the methacrylic acid of EMAA and form ionic crosslinks in the SBS/EMAA blends. The reactions are monitored by characterising **the structure changes** of the mixtures taken out of the internal mixer chamber at three different mixing intervals. The torque-time curve of melt-mixing of SBS/EMAA/Zn (1.5) is shown in **Figure 1**. The dispersion of ZnO (1.5) in the polymer blends caused an increase of the torque with mixing time, three samples were collected corresponding to the unreacted sample *a*, a partially reacted sample *b* and a nearly **completely** reacted sample *c*, as shown in Figure 1. The structures of the three samples were characterized by FTIR and the results are shown in **Figure 2a**. A strong absorbance peak at 1698 cm^{-1} observed in the sample *a* corresponds to the COOH groups in EMAA. Its relative intensity became weaker in sample *b*, and even disappeared in sample *c*. Meanwhile, two new absorbance peaks at 1585 and 1417 cm^{-1} were observed in sample *b* and *c*, attributed to the asymmetric and symmetric stretching modes of carboxylate anion, respectively. And the relative intensity of carboxylate anion absorbance peaks got stronger with prolonging mixing time of the sample. To ensure a completed neutralization reaction, the unreacted sample *a* was further heated up to $170\text{ }^{\circ}\text{C}$ and the infrared spectra were recorded *in situ* (Figure 2b). With prolonging reaction time, the intensity of carboxylate anion absorbance peaks became stronger and the COOH absorbance peak completely disappeared after 30 min at $170\text{ }^{\circ}\text{C}$, indicating a complete reaction.

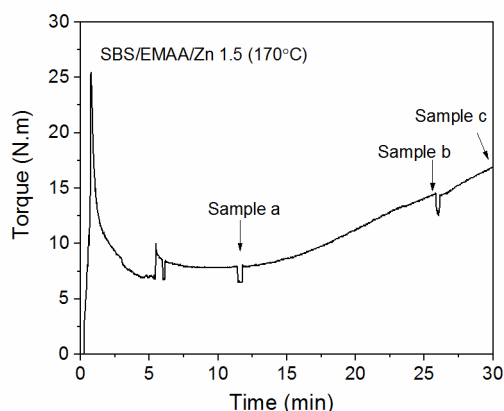


Figure 1. Dynamic shearing mixing curve of SBS/EMAA/Zn (1.5) blend at 170 °C.

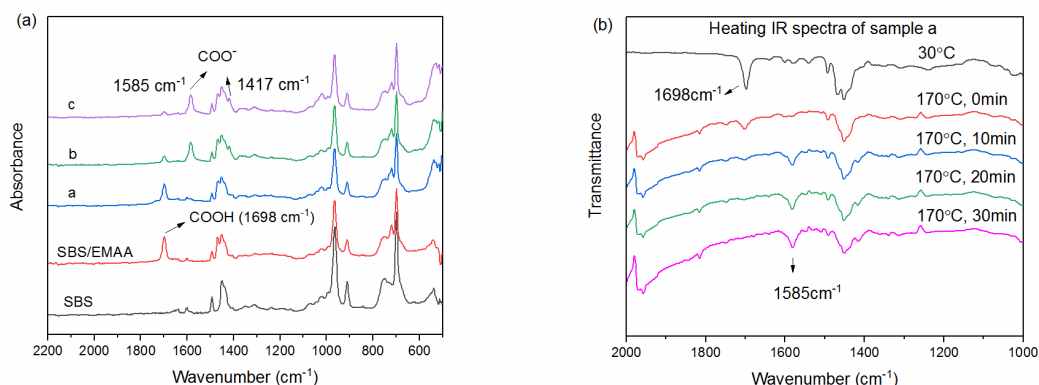


Figure 2. FTIR spectra of SBS/EMAA/Zn (1.5) samples (a) taken at different mixing periods from the mixing chamber; and the (b) *in situ* measurement of sample a at 170 °C for 30 min.

To control the degree of ion crosslinking, the SBS/EMAA blend were melt-mixed with different contents of ZnO particles at 170 °C, and further compression-molded at 190 °C to complete the neutralization and crosslinking reaction. Based on the integrated absorbance ratio of $1585\text{ cm}^{-1}/1698\text{ cm}^{-1}$ of the FTIR spectra, the neutralization degree can be quantified by the infrared ratio method^[21]. The absorbance by the C=O vibration of COOH at 1698 cm^{-1} decreased gradually with neutralization while the absorbance by the COO⁻¹ vibration at 1585 cm^{-1} increased gradually. According to the Beer's law^[22], the absorbance $A = a b c$ is linearly related to the concentration of the functional group, where A is absorbance, a is a constant

related to group and frequency, b is the thickness of absorbance considered as the same for all the samples, and c is the concentration of the group. The sample film of a blend with excessive ZnO was further reacted at 190 °C, and the spectra recorded before and after the reaction were compared and shown in **Figure 3a**. The ratio $A_{1698} / A_{1585} = 1.16$ for the same functional group concentration in the same sample can be obtained. Finally, the neutralization degree of each blend after reaction can be calculated by $A_{1585} \times 1.16 / [A_{1698} + A_{1585} \times 1.16]$ from the normalized spectrum, as shown in Figure 3b. With ZnO contents of 0.5, 1.0, 1.5, 2.5, 5.0, the neutralization degrees were calculated to be 39%, 74%, 88%, 91%, 95%, and the zinc cation fractions were 0.9 wt%, 1.7 wt%, 2.0 wt%, 2.1 wt%, 2.2 wt%, respectively. The carboxylic acid groups were not completely neutralized during the sample molding, indicating some of the ZnO particles did not take part in the reactions, even though the ZnO was excessive. The main reason **should be** that the carboxylic acid groups attached on the main chain of EMAA have limited mobility, which hindered the reactions with ZnO particles during the compression-molding process. Moreover, the dispersion and agglomeration of ZnO particles in the matrix also limited the reaction efficiency.

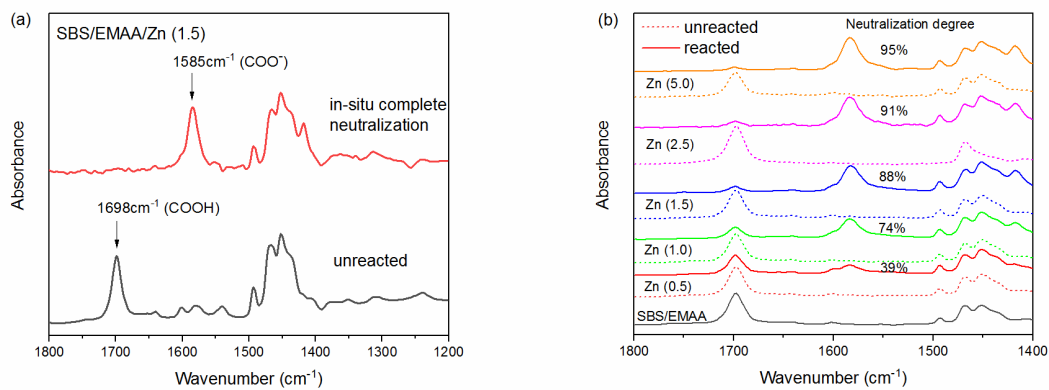


Figure 3. FTIR spectra of SBS/EMAA/Zn (1.5) blend before and after in situ complete neutralization (a), and SBS/EMAA blends with different content of zinc oxide before and after the neutralization reaction.

Figure 4 shows the morphologies of SBS/EMAA/Zn before and after removing the SBS phase. The SBS/EMAA (60/40) blend shows partially co-continuous morphology in Figure 4a, after 1.0 equivalent ZnO was added, the phase morphology became more homogeneous and developed into a typical co-continuous structure (Figure 4b). For the dual-phase structure of polymer blends, EMAA phase has a lower rheological viscosity (as shown in Figure S1), tending to become the continuous phase at the 60/40 component ratio. After the formation of ionic crosslinking among the EMAA chains, the viscosity of EMAA was significantly increased, and the reduced viscosity difference between SBS and EMAA/Zn led to finer co-continuous phase morphology. In Figure 4c, some ZnO particles were observed as a result of the incomplete neutralization reaction as discussed above.

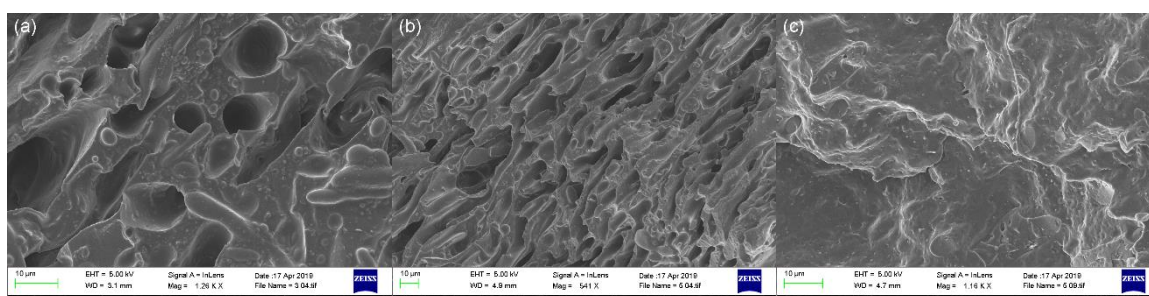


Figure 4. SEM images of (a) SBS/EMAA after etching, (b) SBS/EMAA/Zn (1.0) after etching, and (c) before etching.

3.2. Reinforcement Effect of Ion Crosslinks

The mechanical properties of SBS/EMAA/Zn blends were characterised and shown in **Figure 5**. **The stress at 100% extension** and Young's modulus of the blends are increased with the ZnO content increasing, accompanying decreased elongation at break. A maximum tensile strength of the blends was reached when the ZnO content was 1.0 neutralization equivalent of the acid, corresponding to neutralization degree of 74%. This indicates that it is not necessary to completely neutralise the acid groups of EMAA to reach higher reinforcement, partial neutralization would balance the reversibility and flexibility of the ionic crosslinked structures.

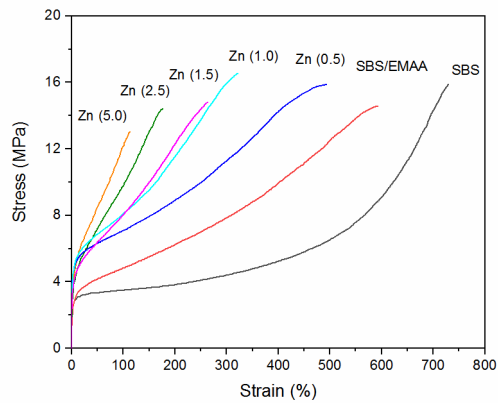


Figure 5. Tensile stress-strain curves of SBS/EMAA blends with different ZnO contents.

The association and disassociation of ionic bonds are temperature-dependent. The reinforcement effect of zinc cations on the blends was investigated by DMTA. The storage moduli of the blends were increased with ZnO contents increasing, especially at high temperatures (**Figure 6**), indicating the improvement of high temperature performance. The glass transition temperatures of EMAA and styrene block in SBS were at 27 °C and 91 °C, respectively, above which the modulus of the SBS/EMAA blend drops abruptly indicating failure in use. For the SBS/EMAA/Zn blends, the formation of zinc ion crosslinks slow down the decrease of the modulus at temperatures over 100 °C, endowing the blends with good elastic performance at high temperatures. Similarly, higher neutralization degree (> 74%) had little effect on the high temperature performance, possibly due to the saturated crosslinking points and low mobility of the polymer chains.

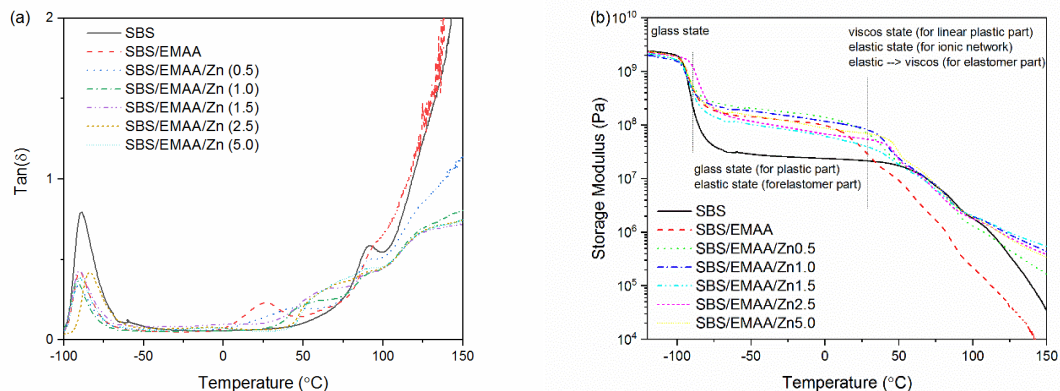


Figure 6. Dependences of $\tan(\delta)$ (a) and storage modulus (b) on temperature for SBS/EMAA blends dynamic mechanical thermal analysis.

The introduction of ion crosslinks to SBS/EMAA also affects the long-time relaxation of the polymers. The rheology measurement of SBS/EMAA at high temperature (150 °C) is shown in **Figure 7**. The modulus of the blend was increased significantly after 74% of neutralization degree, especially for the plateau modulus at low frequencies. The chain entanglements of SBS and the hydrogen bonding interaction of EMAA lead to a second plateau meaning “rubber plateau” in the rheological curve of $G' \sim f$. The introduction of the ionic network further increased the plateau modulus. This liquid-solid transition frequency shifted to high frequency indicating the presence of a strong network, which has been verified in some ion-containing polymers [23, 24]. The crossover frequency of the $G' \sim f$ and $G'' \sim f$ curves can be used to characterise the transition time domain from elastic to viscous behavior. A second crossover frequency at 0.2 Hz and 0.01 Hz appeared for the SBS and SBS/EMAA, respectively, due to the network established by chain entanglements and hydrogen bonding interaction. However, there was no elastic-viscous transition after the introduction of ionic crosslinks, due to the stronger network.

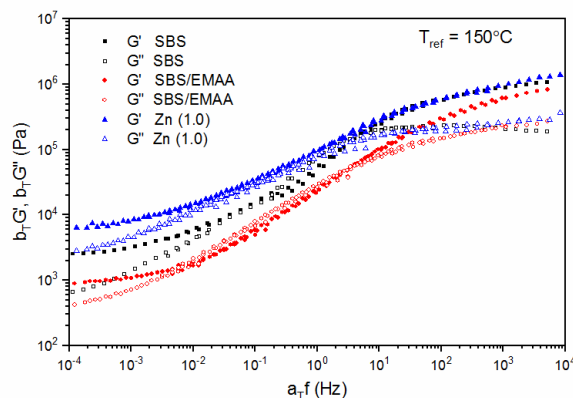


Figure 7. Master curves of storage modulus (G') and loss modulus (G'') as a function of frequency for SBS/EMAA blends at the reference temperature of 150 °C.

3.3. Shape Memory Effect

Shape memory effect of a polymer is a viscoelastic behavior involving the abilities to fix a temporary shape and then to recover the original shape. Under different external conditions, the dominant viscous or elastic behavior of the polymer promotes the transformation. **This effect has been reported to develop new smart materials^[25]**. The glass transition temperature (T_g) or the melting temperature (T_m) plays a significant role in shape memory of polymer and normally can be used as the transition switch. At temperatures above T_g or T_m , polymer chain segments possess good mobility, enabling changes in conformation, and below T_g or T_m , chain segment motion is restricted, enabling to fixing the temporary shape. The styrene block of SBS shows a glass transition at 91 °C, which can be used as the switch even though the transition and the physical crosslinking effect of styrene block are very weak. The introduction of EMAA can potentially promote the shape memory effect of SBS, utilising the melt-crystalline transition of EMAA to help fixing the temporary conformation of SBS, and the formation of the ionic crosslinks can promote the recovery ability.

EMAA has two melting peaks at 65 °C and 98 °C, respectively, corresponding to different crystalline regions, and one crystallization peak at 55 °C, **as shown in Figure 8**. During the second heating scan in the DSC measurement, the two melting peaks merged into one wide peak. The melting temperatures of EMAA were decreased and the crystallization temperature increased in the SBS/EMAA blend, due to imperfect crystalline region. Lower melting temperature benefits a lower switch temperature and higher crystallization temperature enables a faster shape fixing while cooling, which are both in favour of promoting the shape memory effect of SBS. After ZnO was introduced into the blends, the melting and crystallization behavior **changed very little**. Once the neutralization reaction was performed, the two melting peaks in the first heating scan shifted towards each other, and both the melting (and

crystallization) temperature and enthalpy decreased, which might be due to the restriction of mobility of the polymer chains by the ionic crosslinks.

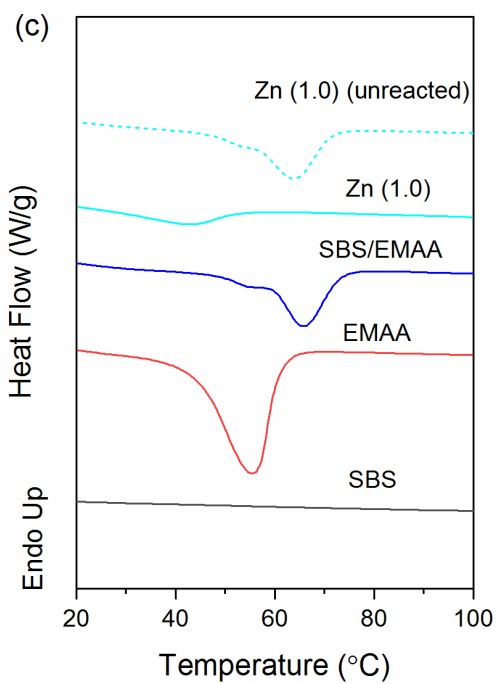
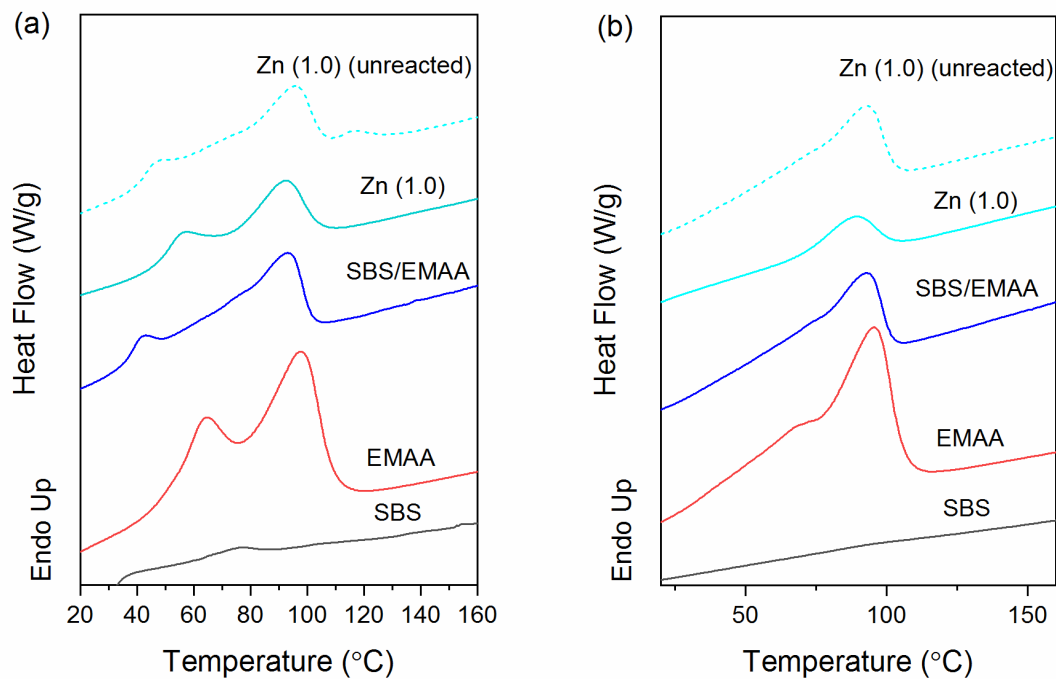


Figure 8. DSC scanning curves of SBS/EMAA blends before and after neutralization reaction. (a) First heating scan; (b) Second heating scan; (c) Cooling scan.

While investigating the shape memory effect of polymers, the deformation and recovery temperature is typically set as $T_{\text{trans}} + 20\text{ }^{\circ}\text{C}$ and the fixing temperature is $T_{\text{trans}} - 20\text{ }^{\circ}\text{C}$ [26]. For SBS and the SBS/EMAA blend, when the specimen was stretched at $100\text{ }^{\circ}\text{C}$, a thin neck appeared due to the deformation of SBS at high temperature and resulted in a small stress. Thus, $80\text{ }^{\circ}\text{C}$ was selected as the deformation and recovery temperature, and the maximum strain was controlled as 40%. The shape memory cycle was shown in **Figure 9a** and the experimental curves of the SBS/EMAA blends were shown in Figure 9b. The shape fixity ratios (R_f) of SBS, SBS/EMAA and SBS/EMAA/Zn (1.0) were 90.2%, 93.3% and 93.3%, respectively, and their shape recovery ratios (R_r) were 56.5%, 77.0% and 84.2%, respectively. After introduction of EMMA and the ionic crosslinks, the shape fixing ability was only slightly improved, but the shape recovery ability was greatly improved. This improvement is mainly due to the reversible ionic crosslinking network constituted by zinc cations and carboxylic acid anions.

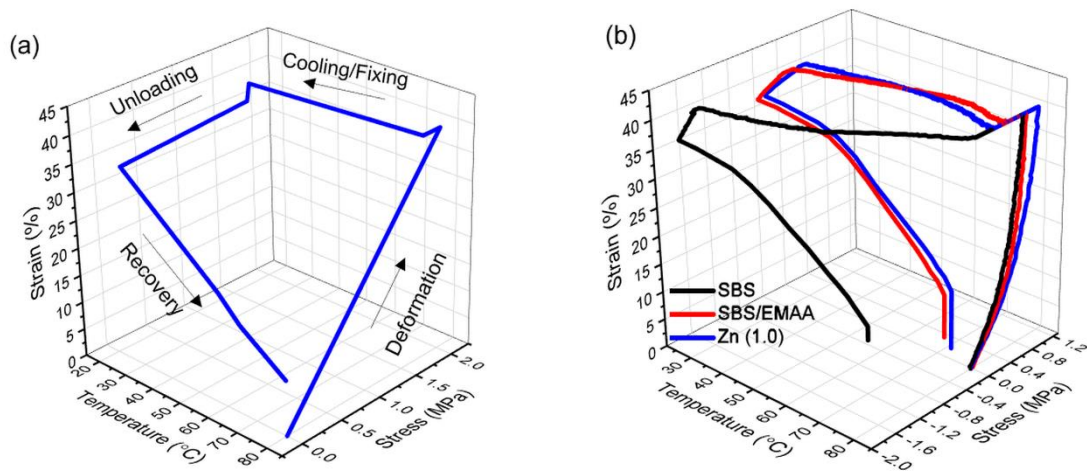


Figure 9. 3D schematic diagram of (a) shape memory cycle and (b) shape memory stress – strain – temperature curves of SBS/EMAA and SBS/EMAA/Zn (1.0) blends.

In comparison with the shape memory effect at small deformation, SBS showed poor shape fixing ability but good recovery efficiency at large strain (200%) and room temperature in the cyclic tensile experiments (**Figure 10**). After one loading-unloading cycle at room temperature, notable residual strains were observed even without long fixing time, which were 15%, 28% and 44% for SBS, SBS/EMAA and SBS/EMAA/Zn (1.0), respectively. Moreover, significantly larger hysteresis was observed for SBS/EMAA (with a dissipating energy of 4.8 MJ m⁻³) and SBS/EMAA/Zn (1.0) (with a dissipating energy of 9.0 MJ m⁻³) compared with that of SBS (with a dissipating energy of 1.2 MJ m⁻³). Besides the elastic chain entanglements of SBS, the energy dissipation related to the hysteresis was originated from the breaking of reversible hydrogen bonds between the carboxyl groups in SBS/EMAA, as well as reversible hydrogen bonds and ionic bonds for SBS/EMAA/Zn (1.0), while loading at large strain. When the specimen was allowed to relax at room temperature without loading, the residual strain decreased. The recovery process involves competition between the elasticity of the elastic chain and the strength of the temporarily re-formed reversible bonds ^[13]. Once the specimen was unloaded, the deformed internal structures (elastic chains, hydrogen bonds and ionic bonds) began to recover, therefore the recovery efficiency increased after introduction of hydrogen or ionic bonds, although the recovery rate was decreased at room temperature due to the sequentially increasing binding energy from chain entanglements, hydrogen bonds to ionic bonds.

After a short holding time (0 min) and a relatively long holding time (10 min) at room temperature, the residual strain recovery ratios for SBS were 13% and 37%, respectively, 34% and 71% for SBS/EMAA, and 44% and 70% for SBS/EMAA/Zn (1.0). After heat treatment at 100 °C for 30 min, the residual strain was completely recovered. However, the stress at 200% extension and the dissipating energy were not completely recovered, and the recovery ratios decreased sequentially from SBS, SBS/EMAA to SBS/EMAA/Zn (1.0). This could be due to

the irreversible deformation under large strain conditions. Similar to those obtained from the shape memory experiments at small strain, the results above indicate that the introduction of EMAA and ionic bonds lead to improved strain fixing and recovery ability.

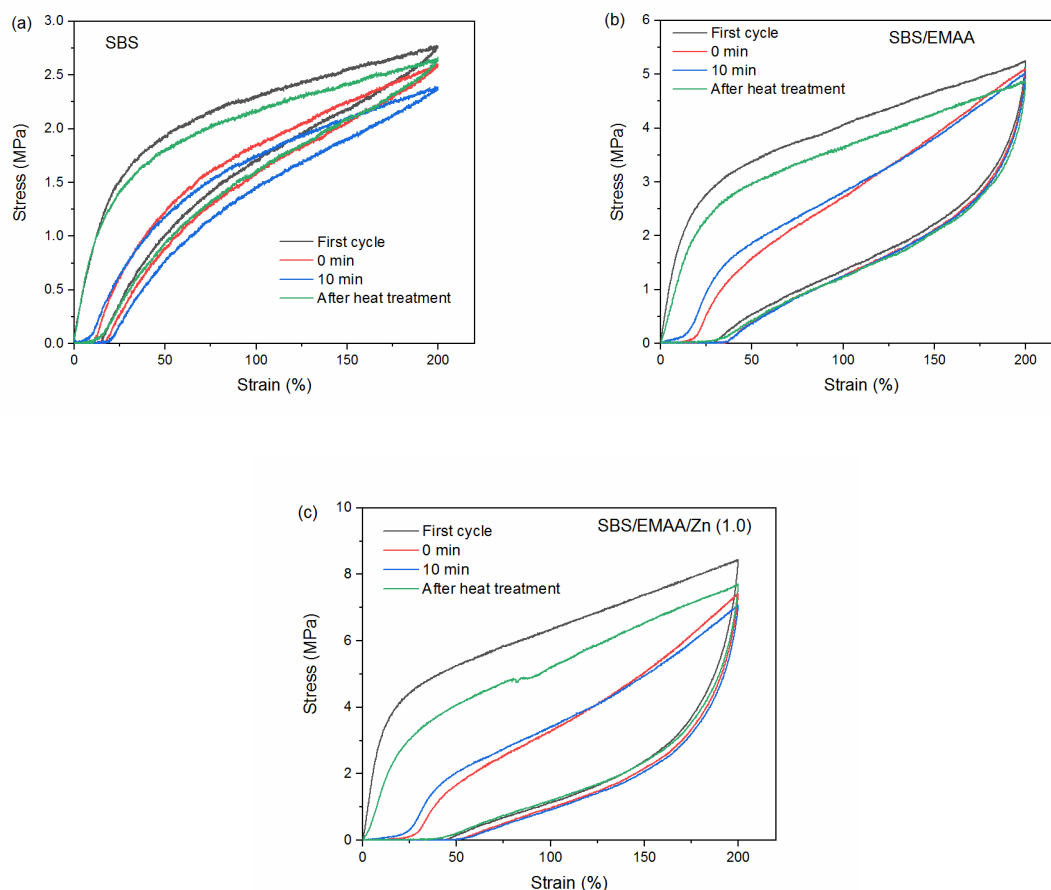


Figure 10. Cyclic tensile stress-strain curves of (a) SBS, (b) SBS/EMAA and SBS/EMAA/Zn (1.0).

Table 1. Effects of EMAA and ionic bonds on the cyclic tensile behavior of SBS.

Sample	Dissipating energy (MJ m^{-3})	Fixing ratio (%)	Recovery ratio (%)				
			Strain		Stress at 200% strain	Energy	
First cycle	First cycle	First cycle	0 min	10 min	30 min at 100 °C	30 min at 100 °C	30 min at 100 °C

SBS	1.2	7.5	13	37	100	96	94
SBS/EMA A	4.8	14	34	71	100	93	88
SBS/EMA A/Zn (1.0)	9.0	22	44	70	100	91	77

3.4. Self-healing Behavior

In the self-healing experiments, the tensile specimen was cut 80~90% of the width, then the damaged surfaces were closed and left to heal at 100 °C for 1 h and 24 h, respectively. **The specimens without healing showed obvious broken crack, but the broken crack completely disappeared for the specimens healed for 24 h (Figure 11).** The stress-strain curves of SBS/EMAA and SBS/EMAA/Zn (1.0) before and after self-healing were shown in **Figure 12**. The total acid content of SBS/EMAA blend is calculated as 3.1 mol%, in the range of 5 mol% as reported by N. Hohlbein^[27]. All the blends showed a self-healing behavior. The self-healing efficiency was quantitatively evaluated by the ratio of the healed to the original samples in terms of tensile strength and elongation at break. The self-healing efficiencies of strength and elongation at break were 32% and 11% for SBS/EMAA, respectively, and 36% and 20% for SBS/EMAA/Zn (1.0), respectively, all higher than those of SBS (about 8% and 9%, respectively). It indicated that the introduction of EMMA and partially neutralized EMMA were capable of improving the self-healing performance of SBS. After the introduction of ionic bonds, the healing efficiency at short time scale were improved (**Figure S2 and S3**). As the healing time extended, the healing efficiency of SBS/EMAA showed little difference from those of SBS/EMAA/Zn blend, due to the long-time aging effect on double bonds of SBS. Overall, the introduction of ionic bonds imparts a faster healing rate to SBS/EMAA, but a strong ionic network of SBS/EMAA/Zn can reduce the self-healing ability of the material.

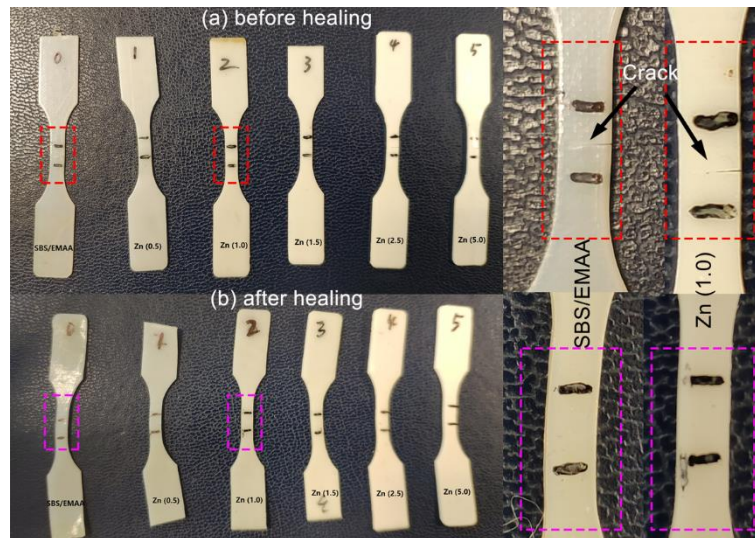


Figure 11. The photos of the specimens without healing (a) and with 24 h healing (b) for SBS/EMAA blends.

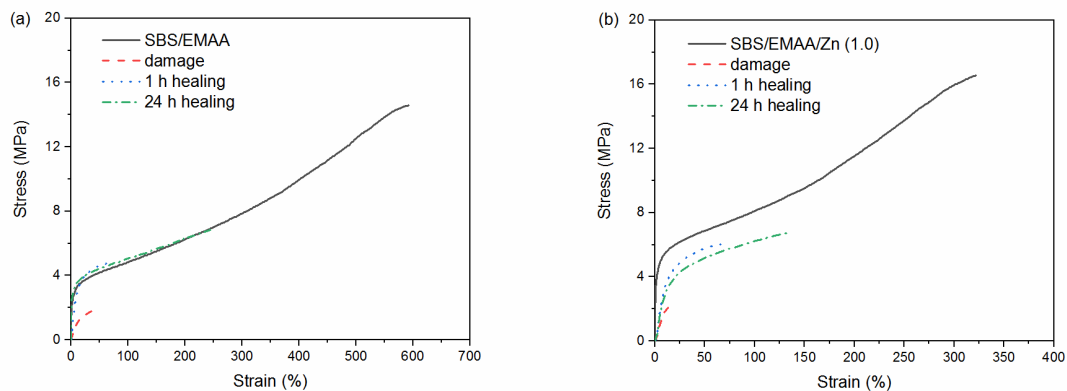


Figure 12. Tensile stress-strain curves of SBS/EMAA (a) and SBS/EMAA/Zn (1.0) (b) before and after self-healing.

4. Conclusions

Ionic bonding was introduced to SBS elastomer by melt-blending with EMAA copolymer and ZnO particles, where the neutralization reaction between the acid groups in EMAA and ZnO particles generate ionic crosslinks in the SBS/EMAA/Zn blends. The relatively low melting temperature of EMAA endowed SBS with better shape memory performance. When the zinc cation based ionic crosslinking network was further introduced through partially neutralizing the carboxyl groups, **the blends showed strong long-time relaxation characteristic and higher**

modulus during rheological tests, indicating significant enhancement effect of ionic bonds. With 74% of the carboxyl groups neutralized, the tensile strength was increased from 14.6 MPa to 16.6 MPa, and the stress at 100% extension was increased from 4.8 MPa to 8.1 MPa. Meanwhile, the shape-fixing ratio and recovery ratio were increased from 90.2% and 56.5% of SBS to 93.3% and 84.2%. When the blend with 74% degree of neutralization was healed at 100 °C for 1 h, the strength and the elongation at break were healed by 36% and 21%, respectively. By this way, the introduction of multiple networks improved the shape memory and self-healing performance of SBS.

Supporting Information

Supporting Information is available from the Wiley Online Library or from the author.

Acknowledgements

Dr W. Wu thanks the funding from China Scholarship Council. The authors also thank The Dow Chemical Company for providing EMAA.

Conflict of Interest

The authors declare no conflict of interest.

[1] S. D. Bergman, F. Wudl, *J. Mater. Chem.* **2008**, *18*, 41.

[2] J. A. Syrett, C. R. Becer, D. M. Haddleton, *Polym. Chem.* **2010**, *1*, 978.

[3] M. Suckow, A. Mordvinkin, M. Roy, N. K. Singha, G. Heinrich, B. Voit, K. Saalwächter, F. Böhme, *Macromolecules.* **2018**, *51*, 468.

- [4] A. M. Grande, L. Castelnovo, L. D. Landro, C. Giacomuzzo, A. Francesconi, M. A. Rahman, *J. Appl. Polym. Sci.* **2013**, *130*, 1949.
- [5] N. García-Huete, W. Post, J. M. Laza, J. L. Vilas, L. M. León, S. J. García, *Eur. Polym. J.* **2018**, *98*, 154.
- [6] C. Xu, L. Cao, B. Lin, X. Liang, Y. Chen, *ACS Appl. Mat. Interfaces* **2016**, *8*, 17728.
- [7] C. Xu, L. Cao, X. Huang, Y. Chen, B. Lin, L. fu, "Self-Healing Natural Rubber with Tailorable Mechanical Properties Based on Ionic Supramolecular Hybrid Network", 2017.
- [8] A. Sallat, A. Das, J. Schaber, U. Scheler, E. S. Bhagavatheswaran, K. W. Stöckelhuber, G. Heinrich, B. Voit, F. Böhme, *RSC Adv.* **2018**, *8*, 26793.
- [9] A. Das, A. Sallat, F. Böhme, M. Suckow, D. Basu, S. Wießner, K. W. Stöckelhuber, B. Voit, G. Heinrich, *ACS Appl. Mat. Interfaces* **2015**, *7*, 20623.
- [10] J. Dahlke, R. K. Bose, S. Zechel, S. J. Garcia, S. van der Zwaag, M. D. Hager, U. S. Schubert, *Macromol. Chem. Phys.* **2017**, *218*, 1700340.
- [11] Y. Peng, Y. Yang, Q. Wu, S. Wang, G. Huang, J. Wu, *Polymer* **2018**, *157*, 172.
- [12] D. Mozhdghi, S. Ayala, O. R. Cromwell, Z. Guan, *J. Am. Chem. Soc.* **2014**, *136*, 16128.
- [13] J. Liu, J. Liu, S. Wang, J. Huang, S. Wu, Z. Tang, B. Guo, L. Zhang, *J. Mater. Chem. A* **2017**, *5*, 25660.
- [14] C. Xu, X. Huang, C. Li, Y. Chen, B. Lin, X. Liang, *ACS Sustain. Chem. Eng.* **2016**, *4*, 6981.
- [15] C. Xu, J. Nie, W. Wu, L. Fu, B. Lin, *Carbohydr. Polym.* **2019**, *205*, 410.
- [16] S. J. Kalista, T. C. Ward, Z. Oyetunji, *Mech. Adv. Mater. Struct.* **2007**, *14*, 391.
- [17] M. A. Rahman, G. Spagnoli, A. M. Grande, L. Di Landro, *Macromol. Mater. Eng.* **2013**, *298*, 1350.
- [18] M. A. Rahman, M. Penco, I. Peroni, G. Ramorino, A. M. Grande, L. Di Landro, *ACS Appl. Mat. Interfaces* **2011**, *3*, 4865.

- [19] M. A. Rahman, M. Penco, I. Peroni, G. Ramorino, G. Janszen, L. Di Landro, *Smart Mater. Struct.* **2012**, *21*, 035014.
- [20] Y. Zhang, H. Li, C. Li, X. Chen, A. Lesser, *Polym. Eng. Sci.* **2019**, *59*, E367.
- [21] K. Han, H. L. Williams, *J. Appl. Polym. Sci.* **1989**, *38*, 73.
- [22] M. M. Coleman, P. C. Painter, *J. Macromol. Sci. C.* **1976**, *16*, 197.
- [23] Q. Chen, Z. Zhang, R. H. Colby, *J. Rheol.* **2016**, *60*, 1031.
- [24] Q. Chen, C. Huang, R. A. Weiss, R. H. Colby, *Macromolecules.* **2015**, *48*, 1221.
- [25] J. Wang, Q. Zhao, H. Cui, Y. Wang, H. Chen, X. Du, *J. Mater. Chem. A* **2018**, *6*, 24748.
- [26] C. Liu, H. Qin, P. Mather, "Review of progress in shape-memory polymers", 2007.
- [27] N. Hohlbein, A. Shaaban, A. R. Bras, W. Pyckhout-Hintzen, A. M. Schmidt, *Phys. Chem. Chem. Phys.* **2015**, *17*, 21005.